International Journal of Science and Research (IJSR)
ISSN: 2319-7064
Impact Factor 2024: 7.101

Synthesis and Characterization of Boron-Doped ZnO Thin Films Using a Novel Spray CVD Technique

S. C. Yadav[1], M. D. Uplane[2]

[1]Department of physics, Miraj Mahavidyalaya, Miraj, Sangli 416410, Maharashtra India
Email: *scyadav12[at]gmail.com*

[2]Department of Instrumentation Science, Savitribai Phule, Pune University, Pune 411 007, Maharashtra, India

Abstract: ***This study presents the successful synthesis of Boron-doped Zinc Oxide (ZnO:B) thin films using a newly developed spray Chemical Vapor Deposition (CVD) technique at low substrate temperatures. The objective is to explore the effects of boron doping concentration and film thickness on the structural, morphological, optical, and electrical properties of ZnO thin films. Characterization was conducted using XRD, FESEM, AFM, UV-Vis spectroscopy, Hall Effect measurements, and photoluminescence spectroscopy. The optimized doping concentration (0.8 at%) demonstrated enhanced crystallinity, improved optical transmittance (~90%), and reduced resistivity (~7.7×10^{-3} Ω·cm), making the films suitable for applications in optoelectronics and transparent conductive devices.***

Keywords: ZnO, Boron doping, Spray CVD, Thin films, Optical properties

1. Introduction

Zinc oxide (ZnO) is a widely studied II–VI semiconductor with a direct wide band gap (~3.37 eV) and high exciton binding energy (~60 meV), making it a promising material for applications in optoelectronics, transparent conducting electrodes, gas sensors, and solar cells [1, 2]. However, the high intrinsic resistivity and instability of undoped ZnO films in ambient conditions—due to oxygen chemisorption and limited carrier concentration—restrict their practical performance in device applications [3, 4]. To overcome these limitations, controlled doping with suitable elements is essential to tailor the electrical, optical, and structural properties of ZnO [2, 5]. This study was motivated by the need to develop a simple, scalable, and low-cost technique for producing high-quality doped ZnO thin films with enhanced transparency and conductivity for optoelectronic applications.

Numerous studies have explored group III and group IV dopants such as aluminum, gallium, and indium to enhance the properties of ZnO thin films [2, 6, 7]. While these dopants are effective, their availability, toxicity, or cost may limit industrial-scale deployment. Boron, a lightweight and abundant element, has recently emerged as a promising alternative due to its small ionic radius (0.23 Å) that allows easy substitution into the Zn^{2+} lattice (0.74 Å), potentially offering a controlled modification of ZnO's structural and electronic characteristics [8]. Although a few studies have reported the synthesis of B-doped ZnO using sol-gel, spray pyrolysis, and LP-CVD methods, systematic work on boron doping using a novel low-temperature spray-CVD technique remains limited [9, 10]. The present work builds on these previous efforts, introducing a modified and optimized deposition route while offering insights into both doping concentration and film thickness effects—thereby presenting novelty in both approach and scope.

In this study, we synthesized boron-doped ZnO thin films using a custom-developed spray CVD technique designed to operate at low substrate temperatures. We investigated the impact of boron concentration (0–1.0 at%) and film thickness on the structural, morphological, electrical, and optical properties of the films. XRD confirmed the retention of a polycrystalline wurtzite structure with enhanced c-axis orientation at optimal doping. FESEM and AFM analyses revealed a morphological transition from pyramidal grains to nano-spherical structures with increasing boron content. Electrical measurements showed a significant decrease in resistivity, and optical studies demonstrated up to 90% transmittance with a slight blue shift in the band gap. The optimum performance was achieved at 0.8 at% boron, highlighting the suitability of this doping level for transparent electronic applications.

2. Experimental Procedure

Boron-doped ZnO (ZnO:B) thin films were deposited using a novel spray chemical vapor deposition (spray CVD) technique [11]. For this study, we used analytical-grade zinc acetate dihydrate ($Zn(CH_3COO)_2\cdot2H_2O$) and boric acid (H_3BO_3) were used as the zinc and boron sources, respectively. Methanol served as both solvent and reactive medium due to its low boiling point and compatibility with the CVD system [12]. A 0.075 M solution of zinc acetate was prepared in methanol, and varying atomic weight percentages of boric acid (0.2–1.0 at%, in 0.2 at% increments) were added to achieve different doping concentrations. A total of 200 mL of the precursor solution was used for each deposition cycle. The films were deposited on pre-cleaned glass microscope slides using the custom-built spray CVD system. During deposition, the substrate temperature was maintained at 220°C, and the reaction chamber (core) temperature was fixed at 330°C (603 K) [13]. Other process parameters, such as the spray rate (6 mL/min), nozzle-to-substrate distance (40 cm), and carrier gas flow rate (10 L/min), were held constant across all experiments. The substrate and core temperatures were precisely

controlled using electronic temperature controllers. To ensure safe operation, any hazardous vapours released during thermal decomposition were removed using an exhaust ventilation system. These optimized conditions were used for the systematic synthesis of ZnO:B thin films, which were subsequently characterized to evaluate the influence of boron doping on their structural, optical, and electrical properties.

3. Results and Discussion

The structural properties of boron-doped ZnO (ZnO:B) thin films synthesized via spray CVD were investigated using X-ray diffraction (XRD) as a function of boron doping concentration (0 to 1.0 at%). The XRD patterns (Figure 1 and Figure 2) exhibit distinct diffraction peaks corresponding to the hexagonal wurtzite structure of ZnO, consistent with ICDD card no. 01-080-0075 (a = 3.2498 Å, c = 5.2066 Å) [14]. The dominant (002) peak observed near 34.4° indicates a strong c-axis preferred orientation, typical of ZnO films grown under equilibrium conditions due to the lowest surface energy along this direction [15]. Additional peaks corresponding to (100), (101), (102), (110), (103), (200), and (112) planes confirm the polycrystalline nature of the films [16]. The intensity and sharpness of the (002) peak varied with doping concentration, with the highest intensity observed for 0.8 at% B, suggesting optimal doping conditions that enhance crystallinity. No secondary phases or impurity peaks related to boron or zinc were detected, implying successful substitutional incorporation of B^{3+} ions into Zn^{2+} lattice sites without disrupting the ZnO crystal structure.

The average crystallite size (D) was calculated using the Scherrer equation:

$$D = \frac{k\lambda}{(\beta \cos \theta)} \quad (1)$$

where λ=0.15406 nm is the X-ray wavelength (Cu Kα), β is the full width at half maximum (FWHM), θ is the Bragg angle, and k is a shape factor (typically 0.9). To account for strain-induced broadening, the Williamson–Hall (W–H) method was also applied using the relation [17]:

$$\beta \cos \theta = \frac{k\lambda}{D} + 2\eta \sin \theta \quad (2)$$

where η is the lattice strain. A linear plot of βcosθ vs. sinθ yields the crystallite size from the intercept and the strain from the slope (Figure 3). Crystallite sizes determined using the W–H method were consistently larger than those from the Scherrer formula, as the latter neglects lattice strain and instrumental broadening effects. The calculated structural parameters are presented in Table 1. With increasing B concentration, the crystallite size decreased, suggesting that boron incorporation inhibits grain growth—likely due to reduced surface mobility of adatoms and increased defect density at grain boundaries. This results in films with finer grains and higher density of grain boundaries.

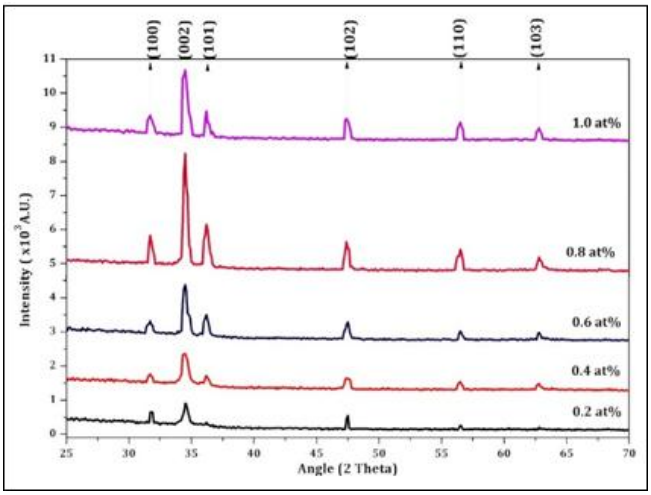

Figure 1: XRD Spectra of varying Boron doping concentration [33]

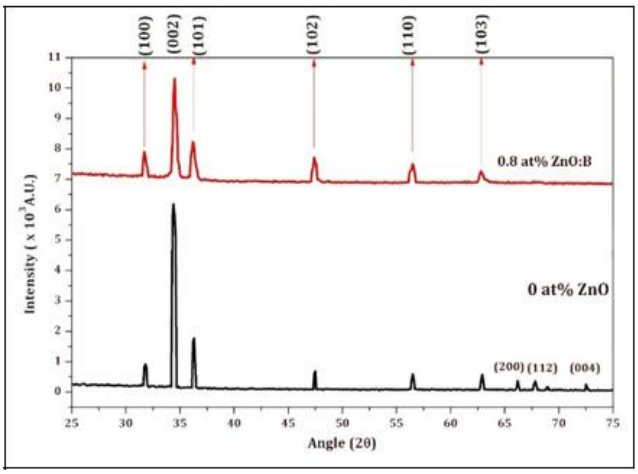

Figure 2: XRD Spectra of intrinsic ZnO and 0.8at% Boron oped ZnO thin films

To quantify internal stress, biaxial tensile stress σ in the ZnO:B films was calculated using the following relation for hexagonal systems [18]:

$$\sigma = -453.6 \times \frac{(c_f - c_b)/}{c_b} \quad (3)$$

where cb=5.209 Å is the c-axis lattice constant of bulk ZnO, and cf is the value calculated from XRD data. All films exhibited positive (tensile) stress, increasing with boron concentration, indicative of compressive strain relaxation through defect formation and grain boundary expansion.

Lattice constants 'a' and 'c' were calculated using the interplanar spacing relation for hexagonal crystals:

$$\frac{1}{d^2} = 4/3 \left[\left(\frac{h^2 + hk + k^2}{a^2} \right] \right. + \frac{l^2}{c^2} \quad (4)$$

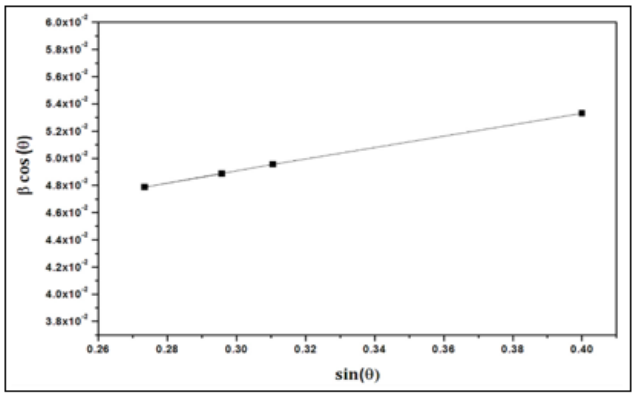

Figure 3: Variation of βcos(θ) vs sin(θ)

Table 1: Structural Parameters of ZnO:B Thin Films at Varying B Concentrations

Doping Concentration	Crystallite Size (nm) (Scherrer)	Crystallite Size (nm) (W–H)	a = b (Å)	c (Å)	Stress (GPa)
0 at%	22	40	3.253	5.211	0.174
0.2 at%	18	38	3.252	5.2039	0.444
0.4 at%	17	37	3.250	5.2037	0.462
0.6 at%	16	30	3.249	5.2032	0.504
0.8 at%	15	21	3.248	5.2031	0.513
1.0 at%	13	20	3.247	5.2028	0.539

The results (Table 4.1) show a gradual decrease in lattice constants with increasing doping concentration, confirming successful B^{3+} substitution due to its smaller ionic radius compared to Zn^{2+}. These results demonstrate that boron doping effectively modifies the microstructure of ZnO thin films by reducing crystallite size, inducing tensile stress, and subtly altering lattice parameters—all of which are essential for tailoring their optoelectronic properties.

The surface morphology of ZnO and boron-doped ZnO (ZnO:B) thin films was examined using field emission scanning electron microscopy (FESEM). The results reveal a pronounced dependence of surface morphology on boron doping concentration. As shown in Figure 4 and Figure 5, the undoped ZnO films exhibited large, well-defined pyramidal grains with a textured surface. These triangular columnar grains are characteristic of preferential c-axis oriented growth in polycrystalline ZnO films [19]. With the progressive incorporation of boron into the ZnO matrix, a significant morphological evolution was observed. The sharp pyramidal structures gradually transformed into smaller, spherical nanograins, and at higher doping concentrations, into petal-like and clustered island morphologies. This transformation indicates that boron doping significantly influences the surface energy dynamics during crystal growth. The observed morphological transition is attributed to the reduced surface mobility of adatoms and an increase in nucleation density due to the smaller ionic radius of B^{3+} compared to Zn^{2+} [20]. The incorporation of boron likely introduces localized lattice distortions and increases the number of grain boundaries, which collectively hinder the growth of larger grains and promote the formation of nanospheres. Higher doping levels resulted in films with finer grains and increased porosity, as evident in the SEM micrographs. This porosity is consistent with the tensile stress observed in XRD analysis, which arises from lattice mismatch and strain accumulation during film growth. The reduction in grain size also contributes to smoother film surfaces and diminished light-scattering properties—favorable for optoelectronic applications where high transparency is required. The boron doping not only alters the structural parameters of ZnO thin films but also plays a pivotal role in tailoring their surface morphology, providing a route for engineering nanostructures with desired properties via the spray-CVD process.

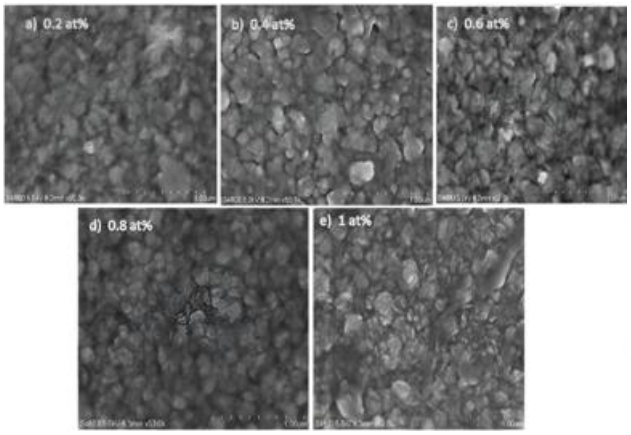

Figure 4: Boron Doping induced different surface morphology in ZnO thin film [33]

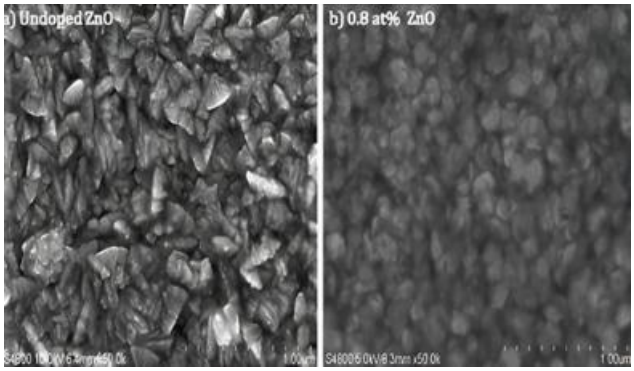

Figure 5: Transition from pyramidal to nano-spherical morphology induced by Boron doping

Atomic Force Microscopy (AFM) was employed to analyse the surface topography of ZnO:B thin films deposited at various boron doping concentrations. The 2D and 3D AFM micrographs (Figure 6 and Figure 7) demonstrate that the film surfaces are uniformly covered with densely packed spherical grains. A clear morphological transition is observed as boron concentration increases—from loosely distributed clusters to well-defined spherical nanograins [21]. The 3D images particularly highlight the progressive reduction in surface roughness with increasing boron content. The film with 0.8 at% B doping exhibited the smoothest surface, indicating an optimized growth condition that enhances surface uniformity. These observations are consistent with FESEM results, which also confirm a transformation from pyramidal to spherical grain morphology. Film thickness and surface roughness were further quantified using a XP-1 stylus surface profiler (Figure 8). An increasing trend in film thickness was observed with higher boron doping levels. This can be attributed to the stronger ionic bonding between boron and oxygen compared to that between zinc and

oxygen. The smaller ionic radius of B^{3+} (0.23 Å) relative to Zn^{2+} (0.74 Å) promotes stronger B–O interactions [22], potentially reducing the evaporation rate during deposition and resulting in greater material accumulation on the substrate [23].

The temperature-dependent electrical behaviour of ZnO:B thin films was examined through two-point probe resistivity measurements in the temperature range 60–300 °C. The Arrhenius plots of ln(ρ) versus 1000/T (Figure 9) reveal two distinct conduction regions:

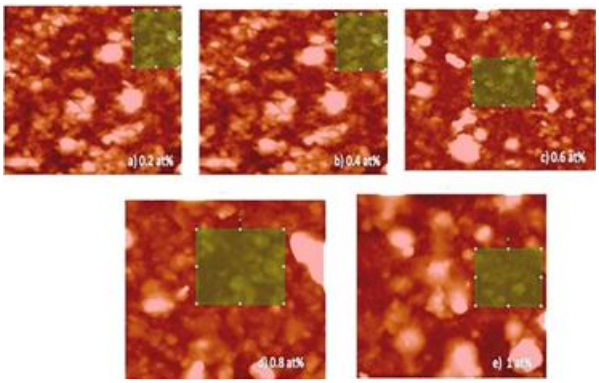

Figure 6: 2D Surface Topography for varying concentration of B doped ZnO thin films

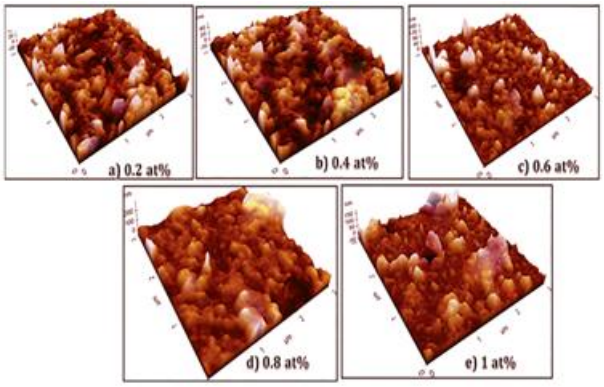

Figure 7: (3D) Surface Topography of B doped ZnO thin films for varying doping concentration [33]

1) A low-temperature region characterized by an exponential decrease in resistivity, and
2) A high-temperature saturation region. This behaviour indicates typical semiconducting characteristics; wherein electrical conductivity increases with temperature. At elevated temperatures, the desorption of oxygen species (O_2^-, O^-) from the film surface reduces the potential barrier at grain boundaries, facilitating charge carrier transport [24]. Additionally, thermal excitation increases the donor density, further contributing to conductivity enhancement [25].

Activation energies for both temperature regions were calculated using the Arrhenius equation [26]:

$$\rho = \rho_0 exp\left(\frac{Ea}{kT}\right) \quad (5)$$

where ρ is the resistivity, Ea is the activation energy (Table 2), k is the Boltzmann constant, and T is the absolute temperature. Across all samples, activation energies in the low-temperature region were consistently lower than those in the high-temperature region. This suggests a shift from extrinsic to intrinsic conduction mechanisms with increasing temperature [27]. In the low-temperature regime, charge transport is likely dominated by thermally activated carriers overcoming shallow donor levels—requiring relatively low activation energies. In contrast, high-temperature conduction is influenced by deeper levels associated with intrinsic defects such as oxygen vacancies (V_O) and zinc interstitials (Zn_i), which demand higher thermal activation.

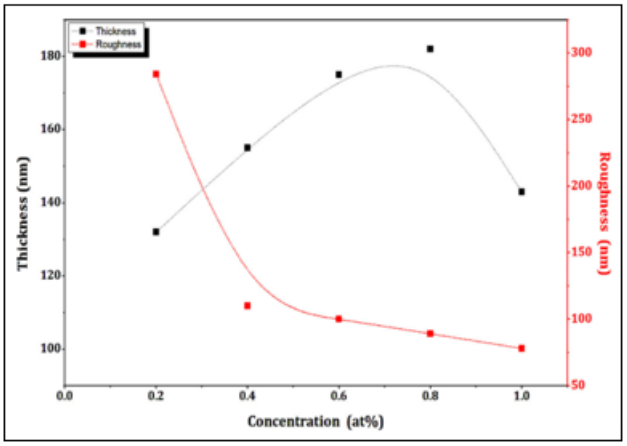

Figure 8: Thickness and Roughness variation of B doped ZnO thin films

Table 2: Activation Energy of ZnO:B Thin Films

Doping Concentration	Activation Energy (eV) Low Temp (60–150 °C)	Activation Energy (eV) High Temp (150–300 °C)
0 at%	0.072	0.190
0.2 at%	0.035	0.180
0.4 at%	0.065	0.660
0.6 at%	0.039	0.350
0.8 at%	0.093	0.170
1.0 at%	0.022	0.280

The optimal electrical performance, indicated by the lowest resistivity and suitable activation energy values, was observed at 0.8 at% boron concentration. This aligns with the previously discussed structural and morphological findings and supports its selection as the optimum doping level for further device applications.

The optical characteristics of boron-doped ZnO (ZnO:B) thin films were evaluated using UV-Visible spectrophotometry in the wavelength range of 360–1000 nm. The transmittance spectra (Figure 10) revealed a clear dependence on boron doping concentration. Films doped with 0.8 at% B exhibited the highest average visible transmittance, reaching approximately 90%. The transmittance spectra of all films showed well-defined interference fringes, indicative of smooth and uniform surfaces with minimal scattering losses. This behaviour suggests a low density of surface and bulk defects, as well as good homogeneity in thickness and refractive index. Compared to the undoped ZnO film, the B-doped films displayed enhanced optical transparency, which correlates with the observed decrease in grain boundary density and smoother surface morphology as evidenced by AFM and FESEM analyses. The improved transparency with increased B doping can be attributed to the reduction in light-scattering centres, enhanced crystallinity, and better film

packing density. Moreover, in transparent conducting oxides like ZnO, the metal-to-oxygen ratio plays a critical role in determining optical transmittance—metal-rich compositions typically lead to reduced transparency due to increased free-carrier absorption [28].

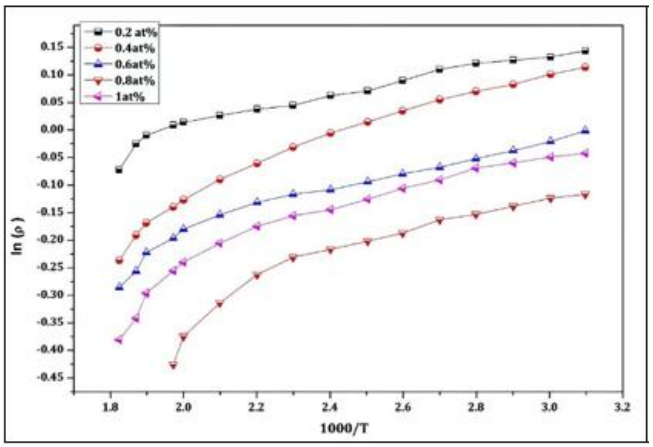

Figure 9: Arrhenius Plot for B doped ZnO thin films

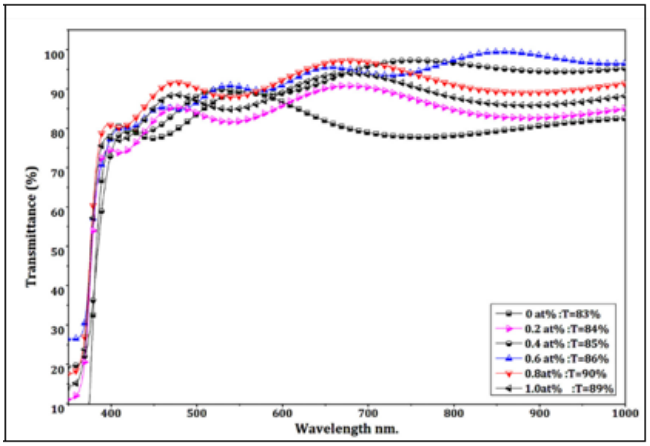

Figure 10: Optical Transmittance of B doped ZnO thin films [33]

The optical absorbance spectra (Figure 11) demonstrated low absorption in the visible and near-infrared regions and high absorption in the UV region for all samples. The absorbance was found to decrease with increasing B concentration, with the 0.8 at% doped film exhibiting the lowest absorption in the visible range—further confirming its superior transparency.

To estimate the optical band gap (Eg), the Tauc relation was used for direct allowed transitions [29]:

$$(\alpha h\nu)^2 = A(h\nu - E_g) \quad (6)$$

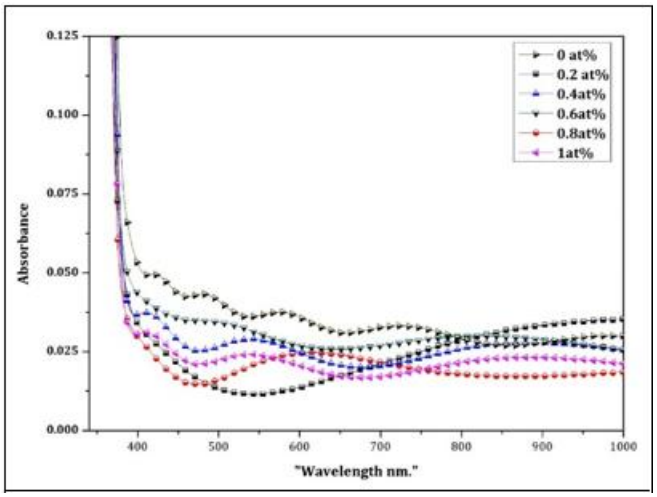

Figure 11: Optical Absorption spectra for B doped ZnO thin films

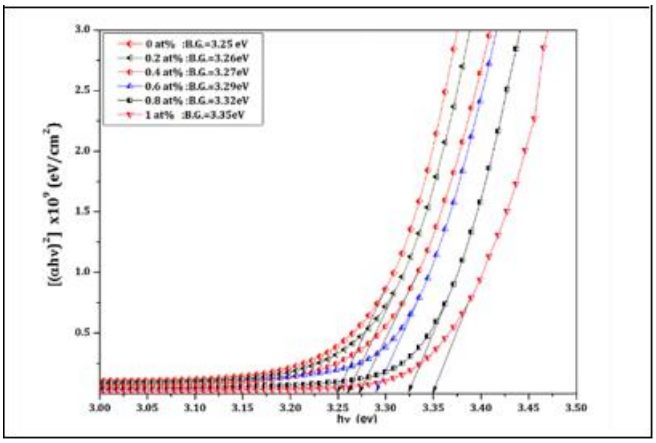

Figure 12; Variation of (αhυ) 2 vs hν for undoped and Boron doping concentration variation in ZnO thin films

where α is the absorption coefficient, hν is the photon energy, and A is a constant. The band gap energy was determined by extrapolating the linear portion of the (αhν)2 versus hν plot to the energy axis (Figure 12). The undoped ZnO film exhibited a band gap of ~3.25 eV [30], which increased to ~3.30 eV at 0.8 at% boron doping. This observed blue shift in band gap with increasing B concentration can be attributed to the Burstein–Moss effect, where the filling of the conduction band by excess carriers leads to an apparent widening of the band gap [31, 32]. Additionally, the reduction in grain size and enhanced quantum confinement effects due to boron incorporation may also contribute to the band gap expansion. Similar trends have been reported in earlier studies on B-doped ZnO thin films deposited via spray pyrolysis.

4. Conclusion

In this study, boron-doped ZnO (ZnO:B) thin films were successfully synthesized using a novel spray chemical vapor deposition (CVD) technique at relatively low substrate temperatures. The effects of boron doping concentration on the structural, morphological, optical, and electrical properties of the films were systematically investigated. XRD analysis confirmed that all films retained a polycrystalline hexagonal wurtzite structure with a preferred (002) orientation. Increasing boron content led to a reduction

in crystallite size and the development of tensile strain, indicating substitutional incorporation of B^{3+} ions into the ZnO lattice. FESEM and AFM studies revealed a distinct morphological transition from pyramidal grains (in undoped ZnO) to spherical and petal-like structures at higher doping levels, with 0.8 at% B yielding the most uniform and smooth surface. Electrical measurements demonstrated semiconducting behaviour across all samples, with the lowest resistivity observed at 0.8 at% boron, attributed to improved crystallinity and increased carrier mobility. Optical studies showed enhanced transmittance and a slight blue shift in the optical band gap (from 3.25 eV to 3.30 eV) with increased doping, consistent with the Burstein–Moss effect and reduced grain size. 0.8 at% boron doping was identified as the optimal concentration, providing the best combination of electrical conductivity, optical transparency, and surface morphology. These findings highlight the potential of spray-CVD-grown ZnO:B thin films as cost-effective, scalable candidates for use in transparent electronics, optoelectronic devices, and solar cell applications.

References

[1] Kumar P., S. Kaushal, S. Kumar, et al. (2025): Recent Advancements in Pure and Doped Zinc Oxide Nanostructures for UV Photodetectors Application. Physica B: Condensed Matter, 417177
[2] Sood S., P. Kumar, I. Raina, et al. Enhancing Optoelectronic Performance Through Rare-Earth-Doped ZnO: Insights and Applications. 12, 454
[3] Wang L., Y. Zhang, X. Wang, et al. (2025): Tunable Electrical Resistivity in Single-Phase VO2 Nanowires Induced by Oxygen Vacancies under Electron Beam Irradiation. Nano Letters
[4] Waqas Alam M., A. Sharma, A. Sharma, et al. (2025): VOC Detection with Zinc Oxide Gas Sensors: A Review of Fabrication, Performance, and Emerging Applications. Electroanalysis **37**, e202400246
[5] Singh K., G. Singh, R. Acevedo, et al. (2025): Recent advancements in ZnO nanoparticles: AI and metaheuristic-enhanced applications in photocatalysis, energy storage, and environmental remediation. Metaheuristics-Based Materials Optimization, 357-383
[6] Marasini S., S. Pandey, R. Ghimire, et al. (2025): Effect of Aluminum Doping on the Optical, Electrical, and Gas Sensing Properties of ZnO Thin Films. Progress in Physics of Applied Materials **5**, 1-9
[7] Nguyen T. H., T. N. L. Pham, T. T. Duong, et al. (2025): Investigation of Ga and F co-doping effects on the electrical, optical, and structural properties of ZnO thin films for transparent electrode applications. Optical and Quantum Electronics **57**, 1-20
[8] Khoreem S. H., A. H. Al-Hammadi, and A. A. M. Othman (2024): Zn2+ ion doping's impact on the vibration spectroscopic properties of higher absorption ions: application to the determination of optical constant properties: advancements in nanotechnology applications. Optical and Quantum Electronics **56**, 466
[9] Karakaya S. and S. Kurtaran (2023): Physical properties of ZnO: B: Ce nanofiber like thin films prepared by ultrasonic spray pyrolysis technique. Inorganic Chemistry Communications **153**, 110747
[10] Yadav S. C. and S. Yadav INDUSTRIAL PURPOSE HIGHLY TRANSPARENT AND LOW RESISTIVE SYNTHESIS OF WELL ORIENTATED B: ZnO THIN FILMS.
[11] Kim B.-H., J.-Y. Lee, Y.-H. Choa, et al. (2004): Preparation of TiO2 thin film by liquid sprayed mist CVD method. Materials Science and Engineering: B **107**, 289-294
[12] Guermoune A., T. Chari, F. Popescu, et al. (2011): Chemical vapor deposition synthesis of graphene on copper with methanol, ethanol, and propanol precursors. Carbon **49**, 4204-4210
[13] Qiao Y., W. Li, S. Chen, et al. (2022): Measurement and calibration of substrate surface temperature in hot filament chemical vapor deposition. Measurement **205**, 112147
[14] Kumar P. and S. N. Reddy (2024): Hydrothermal metal recovery of metal-contaminated wastewater with forest residue: a zero waste discharge process. Environmental Science: Water Research & Technology **10**, 2213-2229
[15] Ţălu Ş., S. Solaymani, N. Tajbakhsh, et al. (2025): Advanced morphological characterization of N: ZnO thin films by RF magnetron sputtering and thermal annealing. Applied Physics A **131**, 1-18
[16] Kaushik V., K. Bhardwaj, D. Kumar, et al. (2024): Effect of various processing parameters on the properties of ZnO thin films. Hybrid Advances **7**, 100295
[17] Alam M. K., M. S. Hossain, N. M. Bahadur, et al. (2024): A comparative study in estimating of crystallite sizes of synthesized and natural hydroxyapatites using Scherrer Method, Williamson-Hall model, Size-Strain Plot and Halder-Wagner Method. Journal of Molecular Structure **1306**, 137820
[18] Chi P.-W., C.-W. Su, and D.-H. Wei (2017): Internal stress induced natural self-chemisorption of ZnO nanostructured films. Scientific Reports **7**, 43281
[19] Debnath D., D. Sen, T. T. Neog, et al. (2024): Growth of ZnO polytypes: multiple facets of diverse applications. Crystal Growth & Design **24**, 871-885
[20] Jellal I., O. Daoudi, K. Nouneh, et al. (2025): Low-temperature growth of highly crystalline ZnO nanopillars by mist chemical vapor deposition technique. International Journal of Modern Physics B, 2550165
[21] Tian X., Y. Sun, H. Li, et al. (2025): Crystallographic Texturing of Electrodeposits for Sustainable Zn Anodes. Advanced Energy Materials **15**, 2403995
[22] Osarumwense E. K., Y. J. Alhaji, and L. M. Bello (2024): Tuning ZnO with Al and B doping for efficient solar cell windows. Journal of Basics and Applied Sciences Research **2**, 15-25
[23] Benli B., E. Tabak, A. Kösemen, et al. Enhanced Photocatalytic and Electrical Performance of Boron-Doped Zno Nanorods: A Taguchi Optimization Approach for Degradation Efficiency. Available at SSRN 5233816
[24] Defferriere T., Y. B. Kim, C. Gilgenbach, et al. (2025): Grain Boundary Space Charge Engineering of Solid Oxide Electrolytes: Model Thin Film Study. arXiv preprint arXiv:2504.10684
[25] Guo M., G. Orr, P. Lan, et al. (2025): Defect dynamics in ZnO varistors under electrical stress: A potential

method to improve electrical properties. Journal of the European Ceramic Society **45**, 117159

[26] Kuzanyan A., A. Sarkisian, N. Aghamalyan, et al. (2025): Magnetoresistance Behavior of Silver-Doped Zinc Oxide Films. physica status solidi (a) **222**, 2400526

[27] Sigalo F. B., H. U. Ogbonda, and C. Oghonda (2023): STIMULATION OF THE EFFECT OF TEMPERATURE ON THE ELECTRICAL CONDUCTIVITY AND CARRIER CONCENTRATION OF INTRINSIC AND EXTRINSIC SEMICONDUCTORS. BW Academic Journal, 13-13

[28] Saeed Z. M., Y. H. Mohammed, and S. M. Ahmad (2024): Atmospheric Pressure Chemical Vapor Deposition Grown One-Dimensional ZnO Nanostructures. Physics of the Solid State **66**, 201-213

[29] Jubu P. R., O. S. Obaseki, D. I. Ajayi, et al. (2024): Considerations about the determination of optical bandgap from diffuse reflectance spectroscopy using the Tauc plot. Journal of Optics, 1-11

[30] Tiss B., D. Martinez-Martinez, C. Mansilla, et al. (2025): Long term degradation kinetics and UV shielding efficiency of TiO2 and ZnO coatings on rubber and cork substrates. Applied Surface Science **695**, 162940

[31] Mahdhi H., N. Haddad, Ş. Ţălu, et al. (2025): Impact of calcium doping on the properties of ZnO thin films: A structural and optical analysis. Journal of Alloys and Compounds **1020**, 179291

[32] Yogamalar N. R. and A. Chandra Bose (2011): Burstein–Moss shift and room temperature near-band-edge luminescence in lithium-doped zinc oxide. Applied Physics A 103, 33-42

[33] Yadav, Sunanda & Uplane, Mahadev. (2012). Synthesis and properties of Boron doped ZnO thin films by spray CVD technique at low substrate temperature. International Journal of Engineering Science.